

Effective thermal conductivity of common geometric shapes

Kyle A. Brucker¹, Joseph Majdalani^{*}

*Department of Mechanical, Aerospace and Biomedical Engineering, University of Tennessee (UTSI),
411 B.H. Goethert Parkway, Tullahoma, TN 37388-9700, United States*

Received 12 April 2005; received in revised form 12 May 2005
Available online 16 August 2005

Abstract

This work explores the porous block paradigm based on replacing an actual heat sink by the volume of fluid that once enveloped the fins. Thermal equivalence is achieved by increasing the thermal conductivity of the lumped fluid above the base plate until the thermal resistance of the actual heat sink is matched. The popularity of the porous block model can be attributed to its ability to approximate the three-dimensional isotherms corresponding to a detailed heat sink. While previous investigations have focused on a numerically calculated, effective thermal property of the compact model, we employ a methodology leading to a closed-form alternative. The explicit solutions that we provide are not limited to the rectangular porous block models used in former studies. Rather, we extend the analysis to cover most fundamental body shapes and flow configurations under both free and forced convection modes. The exact or approximate formulations that we provide apply to most common Nusselt number correlations and obviate the need for guesswork or user-intervention to reach convergence.

© 2005 Elsevier Ltd. All rights reserved.

Keywords: Compact heat sink; Porous fluid block; Extended surface; Flat plate; Coarse model

1. Introduction

The introduction of the microprocessor by Intel Corporation in 1971 has been accompanied by a rapid development of large-capacity memory chips whose packing density has increased from 10 million components in 1990 to 10 billion in 2000 [1]. Pressing demands for size reduction and improved performance of electronic equipment have resulted in the development of

high-power components dissipating significant amounts of heat per unit volume. Since the failure rate of electronic components increases exponentially with operating temperatures, the need for quick thermal-control remedies has gradually become a chief concern in the design and reliability assessment of electronic equipment. This is especially true of electronic enclosures, cabinets, or cases, in which several hundred PCBs, racks, brackets, switches, lights, connectors, control interfaces, and other peripherals have to be packaged. In addition to the daunting task of determining proper cooling loads and solutions, the thermal engineering team is confronted with the need to build a well-designed housing that offers ease of access for replacing failed components, minimizing downtime, and facilitating maintainability.

^{*} Corresponding author. Tel.: +1 931 393 7280; fax: +1 931 393 7333.

E-mail address: maji@utsi.edu (J. Majdalani).

¹ Current address: Department of Mechanical and Aerospace Engineering, University of California, San Diego, La Jolla, CA 92093, United States.

Nomenclature

A_0	$\mu C_p Gr_L$	T_i	inlet coolant temperature
B_0	$a_1 A_0^m$; a_1, m are constants	T_j	junction temperature
C_p	constant pressure specific heat	T_{max}	maximum surface temperature, T_j
g	acceleration due to gravity	T_o	outlet coolant temperature
Gr_L	Grashoff number, $g\beta\Delta TL^3\rho^2\mu^{-2}$	T_s	surface temperature
h	effective heat transfer coefficient	T_∞	ambient coolant temperature
k	thermal conductivity	U	overall heat transfer coefficient, $\dot{Q}/(A\Delta T)$
L	characteristic length	α	thermal diffusivity, $k/\rho C_p$
Pr	Prandtl number, $\mu C_p/k$	β	volumetric thermal expansion coefficient, $1/T_f$
Ra_L	Rayleigh number, $g\beta\Delta TL^3\rho^2\mu^{-2}Pr$	ΔT	$T_s - T_b$
R_T	overall thermal resistance (junction-to-ambient)	μ, ν	dynamic and kinematic viscosities
T_b	bulk mean coolant temperature, $(T_i + T_o)/2$	ρ	density
T_f	film temperature, $(T_s + T_b)/2$		

A number of exotic cooling methods are available today and these are summarized in a survey by Bar-Cohen and Kraus [2]. Generally, these methods rely on a variety of concepts including, but not limited to, free and forced air and liquid cooling, air impingement, liquid immersion, thermoelectric cooling, and heat pipes. So far it appears that the use of heat sinks has been the most widely adopted vehicle for heat removal in populated PCBs. Historically, these compact heat exchangers have been introduced by Kays and London [3] and then carefully explored by Tuckerman and Pease [4]. They continue to receive favor in the works of Goldberg [5], Sasaki and Kishimoto [6], Hwang, et al. [7], Nayak et al. [8], Phillips [9], Gavali et al. [10], Butterbaugh and Kang [11], Visser and Gauche [12], and many others [13].

Heat sinks can be operated under free or forced convective modes depending on the cooling load requirement. Free convection remains the most desirable and deliberate form of cooling being quiet, reliable, simple, and inexpensive. Nevertheless, thermally induced buoyancy currents have not always been adequate in cooling high-density chip packages. Thermal-enhancement techniques are often needed to lower the resistance of a heat sink by increasing its effective surface area beyond the optimal value granted by free convection. To do so, higher fin densities per base plate are needed, and these require better air circulation than is possible naturally. The push or pull air cooling approach is usually resorted to and this is routinely realized through the use of intake and exhaust fans [14].

In its early development, heat sink implementation was slow and expensive as it mostly relied on a blend of theory [13,14] and experimentation [15–17]. With the dramatic growth in computer technology, this focus has shifted to the use of computational fluid dynamics (CFD) [10–14]. The latter has appeared to offer a fast

and reliable alternative, especially when applied to small-scale assemblies.

The adoption of CFD as the method of choice has not been without challenges. Despite modern leaps in processor speed, the discretization demands in modeling increasingly more sophisticated arrays of microchips have been in constant catch-up mode with available computer resources. This is especially true when considering the significant number of boards, pads, high frequency interconnects, and space constraints in designing populated assemblies of multichip modules (MCMs). While a detailed CFD treatment may be practical in analyzing small subassemblies, it clearly becomes overly time-consuming and unaffordable in many applications of real concern.

In order to better cope with the accelerated product development cycles confronting thermal engineers, lumped, coarse, or compact heat sink models have been recently proposed. Examples abound and one may cite the forced convection simulations by Bar-Cohen et al. [18], Krueger and Bar-Cohen [19], Culham et al. [20,21], Linton and Agonafer [22], Butterbaugh and Kang [11], Visser and Gauche [12], Patel and Belady [23,24], Kim and Lee [25], and Narasimhan and Kusha [26]. The same principle has been extended to physical settings involving free convection by Narasimhan and Majdalani [27,28]. All in all, the main idea has been to replace the heat sink with a simpler model that is capable of providing the same thermal and fluid resistance properties exhibited by the actual device. For added convenience, compact modeling has relied on known empirical correlations for predicting flow attributes. Based on the thermal resistance concept, three techniques have been employed so far. These are the ‘boundary condition independent BC-model,’ the ‘flat plate boundary-layer model,’ and the ‘porous block’ or ‘volume resistance model.’

The BC model is based on the notion that a chip package can be characterized by a limited number of well-chosen thermal resistances. At the outset, the model's level of complexity and detail can vary significantly depending on the thermal design requirements. In simple models, a single lumped thermal capacitance is used for each distinct component. In more sophisticated representations, multiple resistors, nodes and shunts can be used in representing top, bottom, side and lead areas that provide passage to heat. The purpose is for the resulting thermal network to provide acceptable approximations for chip temperatures and flow contours. While the original name and formulation must be attributed to Bar-Cohen et al. [18], the BC-approach seems to have evolved from the works of Andrews et al. [29], Andrews [30], and Mahalingam [31]. Since its inception, it has been used by Gautier [32], Le Jannou and Huon [33], Lemczyk et al. [34,35], Lasance et al. [36], and several others.

The flat plate model is also based on an effective thermal resistance concept that has been thoroughly described by Culham et al. [21]. In short, it is implemented by determining the overall thermal resistance R_T from the heat sink and then assigning it either to the base plate, the extended base plate, the raised fin, or the raised fin with base plate assembly.

Instead of assigning the effective thermal resistance to a two-dimensional surface, the porous block model is different in that it distributes R_T uniformly over the three-dimensional volume of fluid that was once occupied by the fins. Following Patel and Belady [23] or Narasimhan and Majdalani [28], reducing the thermal resistance of the volume of fluid above the base plate can be accomplished by artificially increasing its thermal conductivity. An effective thermal conductivity k_e can thus be determined and assigned to the volume of fluid in an attempt to match the overall thermal resistance R_T . Being capable of reproducing three-dimensional temperature maps and heat transfer pathways in an actual heat sink, this approach has been recently adopted by Narasimhan et al. [37].

In forced convection models, an effective pressure loss coefficient needs to be additionally determined in order to account for the flow resistance across the finned space. This problem is further exacerbated by the 'flow bypass effect' caused by the presence of complicated flow pathways through and around the heat sink. In practice, this effect is often manifested by the formation of horseshoe vortices around the heat sink. These vortices are attributed to the increased hydraulic resistance resulting from the narrowing down of flow passages. The higher flow impedance causes the cooling fluid to escape through the side or top clearance above the fin tips following the path of least resistance [25]. Inevitably, the flow bypass effect becomes significant in unducted heat sinks where no shroud is available to suppress the flow

bypass. Studies aiming at improving the prediction of hydraulic loss coefficients include those by Souza et al. [15], Vogel [16], Wirtz et al. [17], Butterbaugh and Kang [11], Patel and Belady [23], Teertstra et al. [38], and Narasimhan et al. [39]. In the free convection models examined by Narasimhan and Majdalani [27,28], calculating the small pressure loss in the detailed heat sink simulation has posed a lesser challenge. Conversely, determining the effective thermal conductivity has been considerably more difficult due to the increased algebraic complexity of empirical correlations for buoyancy-driven flows.

It should be noted that, throughout these studies, standard heat transfer correlations have been used in calculating equivalent thermal properties. This is especially true of porous block models that require evaluating the effective thermal conductivity k_e of the detailed heat sink. In previous investigations, k_e had to be determined numerically from standard heat transfer correlations (e.g., those by Churchill and Chu [40]) for laminar and turbulent flow over a flat plate. Furthermore, applications have been limited to tetrahedral heat sinks that give rise to rectangular porous blocks. In reality, electronic cooling applications involve a diverse mix of geometric configurations, sizes, shapes, and orientations. In cylindrical heat sinks, for example, base plates have circular cross-sections. Since non-rectangular heat sinks and base plates have not been considered in compact heat sink modeling, it is the intent of this article to present closed-form solutions for the effective thermal conductivity of geometric configurations that could be encountered in industrial units. To that end, we will seek either exact or asymptotic solutions for those cases in which k_e has been iteratively determined in previous studies. It is hoped that the direct solutions for k_e will obviate the need for numerical root solving, bracketing, and user-intervention. Considering that the operating environment for compact heat sinks is not known beforehand, the explicit solutions that we seek for k_e will be presented in a general form to facilitate portability. After covering the widely used rectangular geometry, our approach will be extended to other physical configurations that constitute the building blocks of complex heat sinks. In this vein, the forthcoming analysis will encompass both free and forced convection modes under laminar, turbulent and combined flow regimes.

2. The equivalent thermal resistance

In order to ensure that the overall thermal resistance of a compact model matches that of a detailed heat sink, a few steps must be carried out before the effective thermal conductivity of the corresponding porous block can be determined. The key is to obtain the overall heat

transfer coefficient characterizing the actual heat sink. These steps are described in several articles including those by Patel and Belady [23], Kim and Lee [25], and Narasimhan and Majdalani [28]. They are summarized here for the sake of clarity.

The key step consists of calculating the overall thermal resistance R_T of the actual heat sink. This parameter is an important figure-of-merit used in characterizing the efficacy of competing chip layouts [36]. For a constant heat dissipation rate \dot{Q} , it is calculated from $R_T = \Delta T / \dot{Q}$. The temperature excess $\Delta T = T_{\max} - T_b$ is based on the maximum surface temperature T_{\max} and the coolant temperature T_b . In free convection studies, T_b can be equated to the ambient temperature T_∞ . To find R_T , T_{\max} is conveniently acquired from a detailed heat sink solution. It can also be obtained from experimental measurements or theoretical relations available for a similar heat sink. This value is determined only once for a given cooling load \dot{Q} . Thus, as a large-scale system is being developed, only compact properties are calculated and allocated to each heat sink. This allocation is usually based on a preliminary heat sink sizing that results in a simple model. As the mesh remains unmodified, re-initialization is eliminated, and convergence is faster achieved. A flowchart describing the efficacy of compact models in reducing turnaround times is provided by Patel and Belady [23]. Surely, a detailed heat sink simulation is greatly expedited when a validated numerical model is supplied by the vendor (cf. [18]).

Under forced convection conditions, the temperature excess ΔT can be made more sensitive by basing it on the log-mean temperature difference (LMTD) suggested by Kraus and Bar-Cohen [41]. This value can be calculated from $\Delta T = (T_o - T_i) / \ln[(T_s - T_i) / (T_s - T_o)]$, where T_i and T_o represent the inlet and outlet temperatures directly upstream and downstream of the heat sink. The outlet temperature can be obtained from the coolant flowrate \dot{m} , and specific heat C_p , via $T_o = T_i + \dot{Q} / (\dot{m}C_p)$.

Regardless of the technique used in determining R_T , the next step consists of evaluating the overall heat transfer coefficient U between the base plate and surrounding fluid. This is readily obtainable from $U = (R_T A_b)^{-1}$ where A_b is the surface area of the base plate. The use of an overall heat transfer coefficient in the porous block model constitutes a minor departure from the flat plate boundary-layer model where an effective conductance h_e is employed (see [21,10,16]). In the base plate surface model, for example, the Nusselt number correlation for flow over a vertical plate is used to calculate the heat transfer coefficient h_{hs} from an actual heat sink with total surface area A_{hs} . Recalling that the thermal resistance at the base plate is $(h_e A_b)^{-1}$, the equivalent h_e is then calculated by setting $h_e A_b = A_{hs} h_{hs}$. If T_{\max} estimated by the flat plate model is made to coincide with the maximum surface temperature obtained

numerically, both models will then possess the same overall thermal resistance, $R_T = (h_e A_b)^{-1}$. Consequently, one would have $U = h_e$. The symbol U instead of h_e is presently used because $R_T = (U A_b)^{-1}$ combines, in most models, the effects of convection and radiation. This is due to both modes of heat transfer being accounted for in the detailed CFD simulations used by most investigators in the process of evaluating R_T . This is also true of laboratory measurements in which radiation effects are implicitly captured.

Once U is determined, one can proceed to the third and final step of calculating the effective thermal conductivity of the compact model. This step involves substituting U for h_e in an accepted form of the Nusselt number correlation for the specific case at hand. In free convection studies, the archetypical example consists of a laminar buoyancy-driven flow along a vertically oriented base plate. Since the presence of fins is suppressed in the compact representation, the empirical correlation by Churchill and Chu [40] for flow over a vertical plate becomes appropriate. Using standard descriptors, one may write

$$Nu_L = UL/k_e \\ = 0.68 + 0.67 Ra_L^{1/4} [1 + (0.492/Pr)^{9/16}]^{-4/9} \quad (1)$$

where the Rayleigh number is given by $Ra_L = g\beta\Delta TL^3 / (\nu\alpha)$. Customarily, the isothermal surface condition $T_s = T_{\max}$ is used. This assumption is adopted by most thermal analysts to ensure design safety for given cooling load and geometric constraints. In the foregoing relation, all properties are either known or prescribed by the cooling requirement except for k_e . One must also recognize that this effective thermal conductivity is not that of the coolant at film temperature. Rather, it is an artificially adjusted value that must be assigned to the parallelepiped of fluid above the base plate that once enveloped the fins. Hence, by properly increasing the thermal conductivity of the block of fluid above the base plate, its resistance is reduced in a manner to reproduce the same three-dimensional thermal resistance associated with the actually finned heat sink. According to the porous block paradigm, the thermal conductivity of the coolant is locally increased while entering the ‘finned’ space above the base plate. This is done for the purpose of promoting the same overall heat transfer coefficient characterizing the detailed heat sink. The reduced resistance above the base can thus produce gradual temperature variations that mimic the three-dimensional temperature maps projected by a detailed CFD analysis. The porous block approach differs from the flat plate model in which the temperature drop $T_{\max} - T_b$ is applied across the thin base plate.

In the past studies, an iterative approach has been resorted to every time to calculate k_e from (1) by solving the transcendental expression

$$-UL/k_e + 0.68 + 0.67(\rho C_p g \beta \Delta T L^3)^{1/4} (\nu k_e)^{-1/4} \times [1 + (0.492 k_e)^{9/16} (\mu C_p)^{-9/16}]^{-4/9} = 0 \quad (2)$$

In the current work, a direct asymptotic solution for k_e will be proposed such that the need for numerical iterations is eliminated. The same approach will be applied to other fundamental configurations whose effective thermal conductivities have not been evaluated yet.

3. General free convection

The technical literature is filled with empirical correlations aimed at predicting free convection heat transfer from an isothermal body to a quiescent fluid. These correlations vary in complexity from the simplest form, $Nu_L = CRa_L^m$, to the more general form, $Nu_L = a_0 + a_1 Ra_L^m$ [40]. The latter extends over a wider range of Rayleigh numbers and contains two constants a_0 and a_1 that depend on both geometry and flow regime. The leading-order constant a_0 is added to account for thermal diffusion effects as they become increasingly more important at smaller values of Ra_L . Based on boundary-layer theory, m is taken to be $\frac{1}{4}$ or $\frac{1}{3}$ depending on whether the flow is laminar or turbulent [1]. When the cooling fluid is not air, the Rayleigh number is often multiplied by a universal Prandtl number function exhibiting the familiar form $F(Pr) = [1 + (a_2/Pr)^n]^p$. Here, the right-hand side gives the form of F for laminar flow over a flat plate (see [42]). For the sake of generality, this factor can be incorporated by writing

$$Nu_L = a_0 + a_1 Ra_L^m [1 + (a_2/Pr)^n]^{mr} \quad (3)$$

The resulting equation can be used to simultaneously represent free convection over a vertical plate, a horizontal, vertical or inclined cylinder, a cube in several orientations, a sphere, a bisphere, a prolate spheroid, and an oblate spheroid. The constants a_0 , a_1 , a_2 , m , n , and p are given in Table 1.

In addition to (3) a particularly useful form proposed by Churchill and Chu [40] stretches over the entire range of Rayleigh numbers. Using our nomenclature, this correlation can be expressed by

$$Nu_L = \{a_0 + a_1 Ra_L^{m/q} [1 + (a_2/Pr)^n]^{mr/q}\}^q \quad (4)$$

Eq. (4) is appropriate of vertical flat plates, inclined flat plates, vertical or horizontal cylinders, vertical cones, spheres, inclined disks, and sphere-like surfaces. Constants in (4) are listed in Table 1.

In what follows, we present the explicit solution for k_e depending on the equation type. By going from simple to complex, we not only cover a broad range of correlations, but also provide sufficient examples to illustrate the attendant methodology. Such methodology could later be used to derive k_e in those physical settings that are not covered here.

4. Exact k_e for free convection

For a correlation of the type $Nu_L = CRa_L^m$, an exact solution k_e is available directly from

$$k_e = Gr_L \mu C_p [UL / (CGr_L \mu C_p)]^{1/(1-m)} \quad (5)$$

However, when $Nu_L = a_0 + a_1 Ra_L^m$, a solution must be obtained by solving for the meaningful root of

$$a_0 k_e + a_1 (Gr_L \mu C_p)^m k_e^{1-m} - UL = 0 \quad (6)$$

Two special cases arise depending on whether the flow under consideration is laminar ($m = 1/3$) or turbulent ($m = 1/4$). For laminar flow, (6) yields the cubic polynomial

$$k_e^3 + (a_1/a_0)^3 Gr_L \mu C_p k_e^2 - (UL/a_0)^3 = 0 \quad (7)$$

In this instance, the physical root k_e may be determined using Cardano's method [43]. Two possibilities emerge depending on the sign of Cardano's discriminant, $\Delta = (UL/a_0)^6 - [(a_1/a_0)^3 Gr_L \mu C_p]^3 (UL/a_0)^3$. When $\Delta < 0$, a trigonometric root emerges. This is

$$k_e = \frac{1}{3} b_0 (2 \cos \theta - 1) \\ \theta \equiv \frac{1}{3} \cos^{-1} \left(\frac{27}{2} b_1 b_0^{-3} - 1 \right) \\ b_0 \equiv (a_1/a_0)^3 Gr_L \mu C_p, \quad b_1 \equiv (UL/a_0)^3 \quad (8)$$

In the less probable case of $\Delta \geq 0$, an ordinary root is precipitated. One gets

$$k_e = \frac{1}{6} b_2 + \frac{2}{3} b_0^2 b_2^{-1} - \frac{1}{3} b_0 \\ b_2 \equiv \left(108 b_1 - 8 b_0^3 + 12 \sqrt{81 b_1^2 - 12 b_0^3 b_1} \right)^{1/3} \quad (9)$$

The trigonometric root may be safely used in most chip cooling applications where the characteristic length L is on the order of 1 cm or larger. Eq. (9) should be defaulted to under the rare circumstances in which (8) fails.

For turbulent flows, (6) yields a fourth-order polynomial. The meaningful root can be written as

$$k_e = \left[\sqrt{2 + 2(1 + c_1)^{-1/2} - c_1} - 1 - \sqrt{1 - c_1} \right] c_0^{-1} \quad (10)$$

where

$$\begin{cases} c_0 \equiv (a_1/a_0)^4 Gr_L \mu C_p \\ c_1 \equiv 2 \left(\frac{2}{3} c_2 c_3 \right)^{1/3} \left[\left(\frac{2}{3} \right)^{1/3} - 8 c_2^{1/3} c_3^{-2/3} \right] c_0^{-2} \\ c_2 \equiv (UL/a_0)^4 \\ c_3 \equiv \sqrt{81 c_0^4 + 768 c_2} - 9 c_0^2 \end{cases} \quad (11)$$

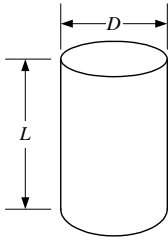
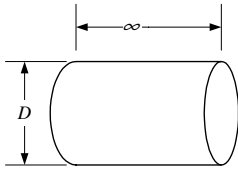
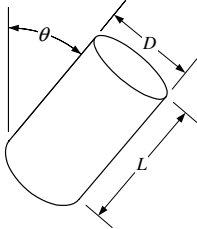
5. Approximate k_e for laminar free convection

The difficulty arises when considering the familiar expression [40]

Table 1
Effective thermal conductivity of common geometric shapes under free convection

Description	Free convection correlation	Effective thermal conductivity
1	$Nu_L = 0.68 + \frac{0.67Ra_L^{1/4}}{(1 + 0.671Pr^{-9/16})^{4/9}}$ laminar, Churchill and Chu [40]	$k_e \rightarrow \text{Eq. (31)}, 10^0 \leq Ra_L \leq 10^9$ $(m, n, p) = (\frac{1}{4}, \frac{9}{16}, \frac{4}{9}), a_i = (0.68, 0.67, 0.492)$ $s_i = (2 \times 10^{-7}, -2 \times 10^{-5}, 0.0012, -0.0465, 1.0311)$
2	$Nu_L = \left[0.825 + \frac{0.387Ra_L^{1/6}}{(1 + 0.671Pr^{-9/16})^{8/27}} \right]^2$ laminar or turbulent, Churchill and Chu [40]	$k_e \rightarrow \text{Eq. (46)}, 10^0 \leq Ra_L \leq 10^{13}$ $a_i = (0.825, 0.387, 0.492)$ $s_i = (2 \times 10^{-7}, -2 \times 10^{-5}, 0.0012, -0.0463, 1.0304)$
3	$Nu_L = 0.59Ra_L^{1/4}$ laminar, McAdams [48]	$k_e = 2.03\sqrt[3]{(UL)^4/(Gr_L\mu C_p)}, 10^4 \leq Ra_L \leq 10^9$
4	$Nu_L = 0.1Ra_L^{1/3}$ turbulent, Warner and Arpaci [49],	$k_e = 31.62\sqrt{(UL)^3/(Gr_L\mu C_p)}, 10^9 \leq Ra_L \leq 10^{13}$
5	$Nu_L = 0.021Ra_L^{2/5}$ turbulent, Eckert and Jackson [50]	$k_e = 1.6 \times 10^{-3}\sqrt{(UL)^5/(Gr_L\mu C_p)^2}, 10^9 \leq Ra_L \leq 10^{13}$
6	$Nu_L = 0.27Ra_L^{1/4}$, hot side down Lloyd and Moran [51]	$k_e = 62.9\sqrt[3]{(UL)^4/(Gr_L\mu C_p)}, 10^5 < Ra_L < 10^{11}$
7	$Nu_L = 0.54Ra_L^{1/4}$, hot side up laminar, Lloyd and Moran [51]	$k_e = 2.274\sqrt[3]{(UL)^4/(Gr_L\mu C_p)}, 10^4 \leq Ra_L \leq 10^7$
8	$Nu_L = 0.15Ra_L^{1/3}$, hot side up turbulent, Lloyd and Moran [51]	$k_e = 0.0581\sqrt{(UL)^3/(Gr_L\mu C_p)}, 10^7 \leq Ra_L \leq 10^{10}$
9	$Nu_L = 0.56(Ra_L \cos \theta)^{1/4}$ $T_f \rightarrow T_c = T_s - 0.25(T_s - T_\infty)$ $\beta = 1/T_\beta, T_\beta = T_\infty + 0.50(T_s - T_\infty)$ laminar, Fujii and Imura [52]	$k_e = 2.166\sqrt[3]{(UL)^4/(Gr_L\mu C_p \cos \theta)}, 10^5 \leq Ra_L \cos \theta \leq 10^{11}, 0^\circ \leq \theta \leq 89^\circ$
10	$Nu_L = \left[0.825 + \frac{0.387Ra_L^{1/6}}{(1 + 0.671Pr^{-9/16})^{8/27}} \right]^2$ laminar or turbulent, Churchill [53]	$k_e \rightarrow \text{Eq. (46)}, \forall Ra_L, g \rightarrow g \cos \theta, \theta \leq 60^\circ$ $a_i = (0.825, 0.387, 0.492)$ $s_i = (2 \times 10^{-7}, -2 \times 10^{-5}, 0.0012, -0.0463, 1.0304)$
11	$Nu_L = 0.17(Gr_L^* Pr)^{1/4}$ $Gr_L^* = g\beta UL^4 \cos \theta / (kv^2)$	$k_e = \left\{ [0.17(g\beta\mu C_p UL^4 \cos \theta / v^2)^{1/4}] / (UL) \right\}^2, 10^{10} < Gr_L^* Pr < 10^{15}$

Table 1 (continued)

Description	Free convection correlation	Effective thermal conductivity
12 	$Nu_L = 0.68 + \frac{0.67Ra_L^{1/4}}{(1 + 0.671Pr^{-9/16})^{4/9}}$ laminar, Churchill and Chu [40]	$k_e \rightarrow \text{Eq. (31)}, 10^0 \leq Ra_L \leq 10^9,$ $D/L \geq 35/Gr_L^{1/4}$ $a_i = (0.68, 0.67, 0.492), (m, n, p) = (\frac{1}{4}, \frac{9}{16}, -\frac{4}{9})$ $s_i = (2 \times 10^{-7}, -2 \times 10^{-5}, 0.0012, -0.0465, 1.0311)$
13	$Nu_L = 3.444 + \frac{0.645Ra_L^{1/4}}{(1 + 0.671Pr^{-9/16})^{4/9}}$ laminar, Yovanovich [54]	$k_e \rightarrow \text{Eq. (31)}, 0 \leq Ra_L \leq 10^8, L = A_w^{1/2}$ $a_i = (3.444, 0.645, 0.492), (m, n, p) = (\frac{1}{4}, \frac{9}{16}, -\frac{4}{9})$ $s_i = (2 \times 10^{-7}, -2 \times 10^{-5}, 0.0012, -0.0465, 1.0311)$
14	$Nu_L = \left[0.825 + \frac{0.387Ra_L^{1/6}}{(1 + 0.671Pr^{-9/16})^{8/27}} \right]^2$ laminar or turbulent, Churchill [53]	$k_e \rightarrow \text{Eq. (46)}, \forall Ra_L, D/L \geq 35/Gr_L^{1/4}$ $a_i = (0.825, 0.387, 0.492)$ $s_i = (2 \times 10^{-7}, -2 \times 10^{-5}, 0.0012, -0.0463, 1.0304)$
15 vertical cylinder	$Nu_L = 0.53Ra_L^{1/4}$ laminar, McAdams [48]	$k_e = 2.02 \sqrt[3]{(UL)^4 / (Gr_L \mu C_p)}, 10^4 \leq Ra_L \leq 10^9$
16	$Nu_L = 0.1Ra_L^{1/3}$ turbulent, Warner and Arpaci [49]	$k_e = 31.62 \sqrt{(UL)^3 / (Gr_L \mu C_p)}, 10^9 \leq Ra_L \leq 10^{13},$ $D/L \geq 35/Gr_L^{1/4}$
17	$Nu_L = 3.444 + \frac{0.683Ra_L^{1/4}}{(1 + 0.671Pr^{-9/16})^{4/9}}$ laminar, Yovanovich [54]	$k_e \rightarrow \text{Eq. (31)}, 10^0 \leq Ra_L \leq 10^9, L = \frac{1}{2}D\pi^{1/2}$ $a_i = (3.444, 0.683, 0.492), (m, n, p) = (\frac{1}{4}, \frac{9}{16}, -\frac{4}{9})$ $s_i = (2 \times 10^{-7}, -2 \times 10^{-5}, 0.0012, -0.0465, 1.0311)$
18 	$Nu_D = 0.36 + \frac{0.518Ra_D^{1/4}}{(1 + 0.721Pr^{-9/16})^{4/9}}$ laminar, Churchill and Chu [55]	$k_e \rightarrow \text{Eq. (37)}, 10^{-6} < Ra_D < 10^9, L = D$ $a_i = (0.36, 0.518, 0.559), (m, n, p) = (\frac{1}{4}, \frac{9}{16}, -\frac{4}{9})$ $s_i = (2 \times 10^{-7}, -2 \times 10^{-5}, 0.0012, -0.0465, 1.0311)$
19	$Nu_D = \left[0.60 + \frac{0.387Ra_D^{1/6}}{(1 + 0.721Pr^{-9/16})^{8/27}} \right]^2$ turbulent, Churchill and Chu [55]	$k_e \rightarrow \text{Eq. (46)}, Ra_D \geq 10^9, L = D$ $a_i = (0.60, 0.387, 0.559)$ $s_i = (2 \times 10^{-6}, -0.0001, 0.0042, -0.087, 1.0298)$
20 horizontal cylinder	$Nu_D = 0.675Ra_D^{0.058}, 10^{-10} \leq Ra_D \leq 10^{-2}$ $Nu_D = 1.02Ra_D^{0.148}, 10^{-2} < Ra_D \leq 10^2$ $Nu_D = 0.85Ra_D^{0.188}, 10^2 < Ra_D \leq 10^4$ $Nu_D = 0.48Ra_D^{0.25}, 10^4 < Ra_D \leq 10^7$ $Nu_D = 0.125Ra_D^{1/3}, 10^7 < Ra_D \leq 10^{12}$ Morgan [56]	$k_e = \{ UL / [0.675(Gr_L \mu C_p)^{0.058}] \}^{1.062}$ $k_e = \{ UL / [1.02(Gr_L \mu C_p)^{0.148}] \}^{1.174}$ $k_e = \{ UL / [0.85(Gr_L \mu C_p)^{0.188}] \}^{1.234}$ $k_e = \{ UL / [0.48(Gr_L \mu C_p)^{1/4}] \}^{4/3}$ $k_e = \{ UL / [0.125(Gr_L \mu C_p)^{1/3}] \}^{3/2}$
21 	$Nu_L = [2.9 - 2.32(\sin \theta)^{0.8}] \times Gr_D^{-1/12} (Gr_L Pr)^{0.1 \sin \theta + 0.25}$ $(Gr_L Pr)_{cr} = 2.6 \times 10^9 + 1.1 \times 10^9 \tan \theta$ laminar, Al-Arabi [57]	$k_e = [ULB^{-1} (Gr_L \mu C_p)^{-1/4 - 0.1 \sin \theta}]^{1.75 - 0.1 \sin \theta}$ $B = 2.9 - 2.32(\sin \theta)^{0.8} Gr^{-1/12}$ $9.88 \times 10^7 \leq Gr_L Pr \leq (Gr_L Pr)_{cr}$ $1.08 \times 10^4 \leq Gr_D Pr \leq 6.9 \times 10^5$
22	$Nu_L = [0.47 - 0.11(\sin \theta)^{0.8}] \times Gr_D^{-1/12} (Gr_L Pr)^{1/3}$ $(Gr_L Pr)_{cr} = 2.6 \times 10^9 + 1.1 \times 10^9 \tan \theta$ turbulent, Al-Arabi [57]	$k_e = \sqrt{(UL)^3 Gr_L^{-3/4} / \{ [0.47 - 0.11(\sin \theta)^{0.8}] \mu C_p \}}$ $(Gr_L Pr)_{cr} \leq Gr_L Pr \leq 2.95 \times 10^{10}$ $1.08 \times 10^4 \leq Gr_D Pr \leq 6.9 \times 10^5$
23 inclined cylinder	$Nu_L = 3.444 + \frac{0.673Ra_L^{1/4}}{(1 + 0.671Pr^{-9/16})^{4/9}}$ $\theta = 45^\circ$, laminar, Yovanovich [54]	$k_e \rightarrow \text{Eq. (31)}, 10^0 \leq Ra_L \leq 10^9, L = A_w^{1/2}$ $a_i = (3.444, 0.673, 0.492), (m, n, p) = (\frac{1}{4}, \frac{9}{16}, -\frac{4}{9})$ $s_i = (2 \times 10^{-7}, -2 \times 10^{-5}, 0.0012, -0.0465, 1.0311)$

(continued on next page)

Table 1 (continued)

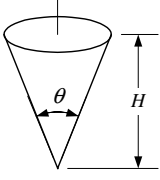
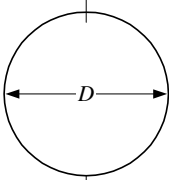
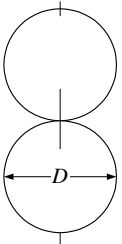
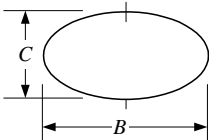
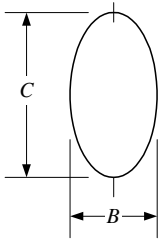
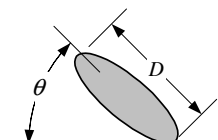
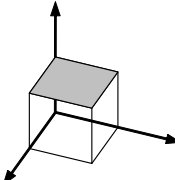
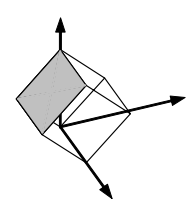
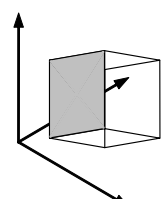
Description	Free convection correlation	Effective thermal conductivity
24	$Nu_L = 0.63(1 + 0.72\varepsilon)Gr_L^{1/4}$ $\varepsilon = 2 \cot(\theta/L)Gr_L^{-1/4}, 0.2 \leq \varepsilon \leq 0.8$	$k_e = 1.6ULGr_L^{-1/4}/(1 + 0.72\varepsilon)$
 vertical cone	laminar or turbulent, Oosthuizen and Donaldson [58]	$3 \times 10^7 \leq Gr_L \leq 5 \times 10^8, 3^\circ \leq \theta \leq 12^\circ$
25	$Nu_L = \left[0.735 + \frac{0.387Ra_L^{1/6}}{(1 + 0.671Pr^{-9/16})^{8/27}} \right]^2$	$k_e \rightarrow \text{Eq. (46)}, \forall Ra_L, L = \frac{4}{3}H$ $a_i = (0.735, 0.387, 0.492)$ $s_i = (4 \times 10^{-7}, -4 \times 10^{-5}, 0.0018, -0.0576, 1.0283)$
26	$Nu_D = 2 + 0.43Ra_D^{1/4}$	$k_e \rightarrow \text{Eq. (53)}, \forall Ra_L, L = \frac{4}{3}H$
27	$Nu_D = 2 + \frac{0.589Ra_D^{1/4}}{(1 + 0.653Pr^{-9/16})^{4/9}}$	$1 < Gr_D < 10^5, Pr \sim 1$ $k_e = \text{Eq. (31)}, Ra_D \leq 10^{11}, Pr > 0.5, L = D$ $a_i = (2, 0.589, 0.469), (m, n, p) = (\frac{1}{4}, \frac{9}{16}, -\frac{4}{9})$ $s_i = (2 \times 10^{-7}, -2 \times 10^{-5}, 0.0012, -0.0465, 1.0311)$
 sphere	laminar or turbulent, Churchill [53]	
28	$Nu_L = \left[1.77 + \frac{0.387Ra_L^{1/6}}{(1 + 0.671Pr^{-9/16})^{8/27}} \right]^2$	$k_e \rightarrow \text{Eq. (46)}, \forall Ra_L, L = \frac{1}{2}\pi D$ $a_i = (1.77, 0.387, 0.492)$ $s_i = (4 \times 10^{-10}, -3 \times 10^{-7}, 6 \times 10^{-5}, -0.0103, 1.0336)$
29	$Nu_L = 3.545 + \frac{0.685Ra_L^{1/4}}{(1 + 0.671Pr^{-9/16})^{4/9}}$	$k_e \rightarrow \text{Eq. (31)}, 0 < Ra_L < 10^8, L = (\frac{\pi}{3})^{1/2}D$ $a_i = (3.545, 0.685, 0.492), (m, n, p) = (\frac{1}{4}, \frac{9}{16}, -\frac{4}{9})$ $s_i = (2 \times 10^{-7}, -2 \times 10^{-5}, 0.0012, -0.0465, 1.0311)$
30	$Nu_L = 3.475 + \frac{0.622Ra_L^{1/4}}{(1 + 0.671Pr^{-9/16})^{4/9}}$	$k_e \rightarrow \text{Eq. (31)}, 0 < Ra_L < 10^8, L = (\frac{2\pi}{3})^{1/2}D$ $a_i = (3.475, 0.622, 0.492), (m, n, p) = (\frac{1}{4}, \frac{9}{16}, -\frac{4}{9})$ $s_i = (2 \times 10^{-7}, -2 \times 10^{-5}, 0.0012, -0.0465, 1.0311)$
 bi-sphere	laminar, Yovanovich [54]	
31	$Nu_L = 3.529 + \frac{0.651Ra_L^{1/4}}{(1 + 0.671Pr^{-9/16})^{4/9}} \quad C/B = 0.5$	$k_e \rightarrow \text{Eq. (31)}, 0 < Ra_L < 10^8, L = A_w^{1/2}$ $a_i = (3.529, 0.651, 0.492), (m, n, p) = (\frac{1}{4}, \frac{9}{16}, -\frac{4}{9})$ $s_i = (2 \times 10^{-7}, -2 \times 10^{-5}, 0.0012, -0.0465, 1.0311)$
 oblate spheroid	laminar, Yovanovich [54]	
32	$Nu_L = 3.342 + \frac{0.515Ra_L^{1/4}}{(1 + 0.671Pr^{-9/16})^{4/9}} \quad C/B = 0.1$	$k_e \rightarrow \text{Eq. (31)}, 0 < Ra_L < 10^8, L = A_w^{1/2}$ $a_i = (3.342, 0.515, 0.492), (m, n, p) = (\frac{1}{4}, \frac{9}{16}, -\frac{4}{9})$ $s_i = (2 \times 10^{-7}, -2 \times 10^{-5}, 0.0012, -0.0465, 1.0311)$

Table 1 (continued)

Description	Free convection correlation	Effective thermal conductivity
33  prolate spheroid	$Nu_L = 3.566 + \frac{0.678Ra_L^{1/4}}{(1 + 0.671Pr^{-9/16})^{4/9}}$ $C/B = 1.93,$ laminar, Yovanovich [54]	$k_e \rightarrow \text{Eq. (31)}, 0 < Ra_L < 10^8, L = A_w^{1/2}$ $a_i = (3.566, 0.678, 0.492), (m, n, p) = (\frac{1}{4}, \frac{9}{16}, -\frac{4}{9})$ $s_i = (2 \times 10^{-7}, -2 \times 10^{-5}, 0.0012, -0.0465, 1.0311)$
34 Sphere-like surface with area A_S and volume ϑ	$Nu_L = \left[\frac{3\pi\vartheta}{A_S} + \frac{0.387Ra_L^{1/6}}{(1 + 0.671Pr^{-9/16})^{8/27}} \right]^2$ laminar or turbulent, Churchill [53]	$k_e \rightarrow \text{Eq. (31)}, \forall Ra_L, L = A_S^{3/2}/(6\vartheta)$ $a_i = (3\pi\vartheta/A_S, 0.387, 0.492)$ $s_i = (4 \times 10^{-10}, -3 \times 10^{-7}, 6 \times 10^{-5}, -0.0103, 1.0336)$
35  inclined disk	$Nu_L = \left[0.748 + \frac{0.387Ra_L^{1/6}}{(1 + 0.671Pr^{-9/16})^{8/27}} \right]^2$ laminar or turbulent, Churchill [53]	$k_e \rightarrow \text{Eq. (46)}, \forall Ra_L, L = \frac{9}{11}D$ $a_i = (0.748, 0.387, 0.492)$ $s_i = (3 \times 10^{-7}, -3 \times 10^{-5}, 0.0017, -0.0553, 1.027)$
36  cube (H^3) with base in plane	$Nu_L = 3.388 + \frac{0.637Ra_L^{1/4}}{(1 + 0.671Pr^{-9/16})^{4/9}}$ laminar, Yovanovich [54]	$k_e \rightarrow \text{Eq. (31)}, 0 < Ra_L < 10^8, L = \sqrt{6}H$ $a_i = (3.388, 0.637, 0.492), (m, n, p) = (\frac{1}{4}, \frac{9}{16}, -\frac{4}{9})$ $s_i = (2 \times 10^{-7}, -2 \times 10^{-5}, 0.0012, -0.0465, 1.0311)$
37  cube oriented 45° to base plane	$Nu_L = 3.388 + \frac{0.663Ra_L^{1/4}}{(1 + 0.671Pr^{-9/16})^{4/9}}$ laminar, Yovanovich [54]	$k_e \rightarrow \text{Eq. (31)}, 0 < Ra_L < 10^8, L = \sqrt{6}H$ $a_i = (3.388, 0.663, 0.492), (m, n, p) = (\frac{1}{4}, \frac{9}{16}, -\frac{4}{9})$ $s_i = (2 \times 10^{-7}, -2 \times 10^{-5}, 0.0012, -0.0465, 1.0311)$
38  cube oriented with diagonal \perp to base plane	$Nu_L = 3.388 + \frac{0.679Ra_L^{1/4}}{(1 + 0.671Pr^{-9/16})^{4/9}}$ laminar, Yovanovich [54]	$k_e \rightarrow \text{Eq. (31)}, 0 < Ra_L < 10^8, L = \sqrt{6}H$ $a_i = (3.388, 0.679, 0.492), (m, n, p) = (\frac{1}{4}, \frac{9}{16}, -\frac{4}{9})$ $s_i = (2 \times 10^{-7}, -2 \times 10^{-5}, 0.0012, -0.0465, 1.0311)$

$$Nu_L = UL/k_e = a_0 + a_1 Ra_L^m [1 + (a_2/Pr)^n]^p \tag{12}$$

which can be obtained by setting $p = mr$ in (3). This relation applies to a number of important shapes whose characteristic constants are furnished in Table 1. In short, the difficulty stems from k_e being simultaneously present in the Nusselt, Rayleigh, and Prandtl numbers. This can be seen by rearranging (12) into

$$UL/k_e = a_0 + a_1 (A_0/k_e)^m \{1 + [a_2 k_e / (\mu C_p)]^n\}^p \tag{13}$$

$$A_0 \equiv \mu C_p Gr_L$$

The power-law embedment of k_e in the universal Prandtl number function eliminates the possibility of obtaining an exact expression for k_e . An asymptotic approximation of the form $k_e \approx k_0 + k_1$ will have to be settled for. To proceed, the Prandtl number function has to be expanded first. Letting $\kappa = a_2/\mu C_p$, it follows that two cases must be considered separately depending on the size of U , and therefore, k_e .

5.1. Type I: Laminar regime, small U case

For small κk_e , one can expand $F(Pr)$ straightforwardly viz.

$$[1 + (\kappa k_e)^n]^p = 1 + p(\kappa k_e)^n + \frac{p(p-1)}{2!} (\kappa k_e)^{2n} + \frac{p(p-1)(p-2)}{3!} (\kappa k_e)^{3n} + \frac{p(p-1)(p-2)(p-3)}{4!} (\kappa k_e)^{4n} + \dots \tag{14}$$

By substituting (14) into (13), one then gathers the multi-order polynomial

$$UL = a_0 k_e + B_0 k_e^{1-m} + C_0 k_e^{1-m+n} + D_0 k_e^{1-m+2n} + E_0 k_e^{1-m+3n} + F_0 k_e^{1-m+4n} \tag{15}$$

where

$$B_0 \equiv a_1 A_0^m$$

$$C_0 \equiv p B_0 \kappa^n$$

$$D_0 \equiv \frac{p(p-1)}{2!} B_0 \kappa^{2n} \tag{16}$$

$$E_0 \equiv \frac{p(p-1)(p-2)}{3!} B_0 \kappa^{3n}$$

$$F_0 \equiv \frac{p(p-1)(p-2)(p-3)}{4!} B_0 \kappa^{4n}$$

It should be noted that, in our search for the most influential term in (15), quantities that are negative have been discounted as they lead to unphysical thermal conductivities. By considering each of the four enumerated terms as leading-order candidates, the zeroth-order expression for k_e is narrowed down to

$$k_e = \left\{ UL/a_0, (UL/B_0)^{1/(1-m)}, (UL/D_0)^{1/(1-m+2n)}, (UL/F_0)^{1/(1-m+4n)} \right\} \tag{17}$$

These terms are plotted in Fig. 1 alongside the numerical solution. This is carried out for three different geometric shapes to ensure portability. From the plot, it is clear that Term 2 has the most influence since it closely approximates the numerical solution. The parameters used in this comparison correspond to a commercial heat sink modeled by Narasimhan and Majdalani [28]. It is characterized by $L = 0.0762$ m, $A_b = 0.00314$ m², $\rho = 1.1$ kg m⁻³, $\mu = 1.95 \times 10^{-5}$ kg m s⁻¹, $C_p = 1007$ J kg⁻¹ K⁻¹, and $T_b = 293.15$ K. By trying other cases, the dominant position of Term 2 is found to be rather independent of this particular choice. Having identified $k_0 = (UL/B_0)^{1/(1-m)}$, the next step is to put

$$k_e^I = (UL/B_0)^{1/(1-m)} + k_1 \tag{18}$$

where the superscript is used to denote a type-I solution. To solve for the first-order correction k_1 , the notion of successive approximations is used. Accordingly, (18) is substituted back into Term 2 of (15) while only the leading-order part k_0 is used in the remaining terms. This permits extracting k_1 from

$$k_1 = -[UL(1-m)]^{-1} (a_0 k_0^2 + C_0 k_0^{2-m+n} + D_0 k_0^{2-m+2n} + E_0 k_0^{2-m+3n} + F_0 k_0^{2-m+4n}). \tag{19}$$

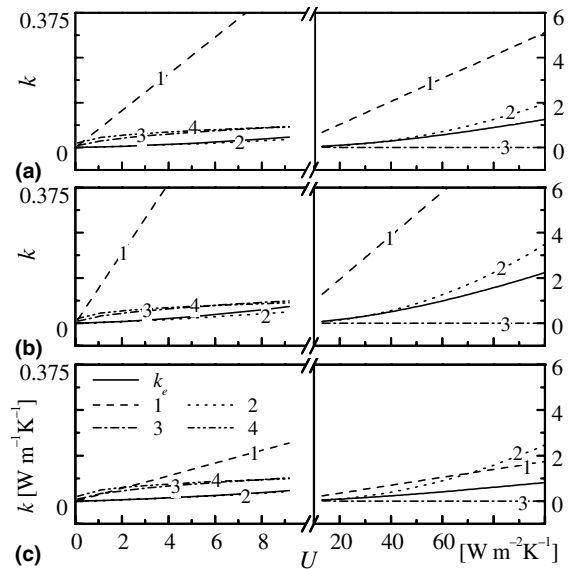


Fig. 1. Relative size of leading terms arising in the expansion of the universal Nusselt number correlation for free convection laminar flow over (a) vertical plates, (b) cylinders, and (c) spheres. Note that while Term 1 dominates for small U , both Terms 1 and 2 are simultaneously needed to evaluate the leading-order term of the large- U approximation.

Eq. (18) is valid for all L and B_0 as long as $0 < k_e^I \leq k_{||}$, where $k_{||}$ is a cut-off value that varies on average between 0.01 and 0.13 $\text{W m}^{-1} \text{K}^{-1}$. This physical limitation is due to the divergence of the Taylor series at larger values of U .

5.2. Type II: Laminar regime, large U case

Recalling that the effective thermal conductivity of the artificial block of fluid is commensurate with the overall heat transfer coefficient of the actual heat sink, the series expansion in (14) can become divergent as U is increased. When κk_e is no longer small, one needs to re-expand (14) in the reciprocal of κk_e . One obtains

$$\begin{aligned}
 & (\kappa k_e)^{np} [1 + 1/(\kappa k_e)^n]^p \\
 &= (\kappa k_e)^{np} \left[1 + p(\kappa k_e)^{-n} + \frac{p(p-1)}{2!} (\kappa k_e)^{-2n} \right. \\
 & \quad \left. + \frac{p(p-1)(p-2)}{3!} (\kappa k_e)^{-3n} + \dots \right] \tag{20}
 \end{aligned}$$

When (20) is substituted back into (13), several terms are precipitated. Some are so small that they can be ignored. The remaining terms are found to be

$$\begin{aligned}
 UL &= a_0 k_e + B_1 k_e^{1+np-m} + C_1 k_e^{1-n+np-m} \\
 & \quad + D_1 k_e^{1-2n+np-m} + E_1 k_e^{1-3n+np-m} \tag{21}
 \end{aligned}$$

where

$$\begin{aligned}
 B_1 &\equiv B_0 \kappa^{np} \\
 C_1 &\equiv B_0 p \kappa^{np-n} \\
 D_1 &\equiv \frac{p(p-1)}{2!} B_0 \kappa^{np-2n} \\
 E_1 &\equiv \frac{p(p-1)(p-2)}{3!} B_0 \kappa^{np-3n} \tag{22}
 \end{aligned}$$

By dismissing negative terms that cannot possibly dominate the solution, three terms are identified in (21) as possible leading-order candidates. These are

$$k_e = \{ UL/a_0, (UL/B_1)^{1/(1+np-m)}, (UL/D_1)^{1/(1-2n+np-m)} \} \tag{23}$$

By comparing these approximations to the exact solution in Fig. 1, one realizes that no single term dominates by itself. Rather, one finds that the leading-order behavior is prescribed by the balance of Terms 1 and 2. Assuming a type-II expansion, $k_e^{II} \approx K_0 + K_1$, the solution must be produced from

$$-UL + a_0 K_0 + B_1 K_0^{1+np-m} = 0 \tag{24}$$

Fortunately, all cases presented in this paper are characterized by a single exponent, $1 + np - m = 1/2$. This simplifying power leads to a quadratic equation. The ensuing two-term expansion for k_e^{II} becomes

$$k_e^{II} = \left[UL + \frac{1}{2} B_1 \left(B_1 - \sqrt{B_1^2 + 4a_0 UL} \right) / a_0 \right] / a_0 + K_1 \tag{25}$$

Using successive approximations, (25) is now substituted into Terms 1 and 2 of (21). However, only K_0 is substituted in all other occurrences of k_e^{II} . Once completed, K_1 is found to be

$$\begin{aligned}
 K_1 &= 16k_0(E_1 + D_1 K_0^{9/16} + C_1 K_0^{9/8}) / (19E_1 + 10D_1 K_0^{9/16} \\
 & \quad + C_1 K_0^{9/8} - 8B_1 K_0^{27/16} - 16a_0 K_0^{35/16}) \tag{26}
 \end{aligned}$$

For the general case of an arbitrary exponent in (24), the correction K_1 takes the form

$$\begin{aligned}
 K_1 &= K_0 (E_1 K_0^{2+2np-2m-3n} + D_1 K_0^{2+2np-2m-4n} + C_1 K_0^{2+2np-2m-5n} \\
 & \quad + B_1 K_0^{4+4np-4m-6n}) / [E_1 (1 + np - m - 3n) K_0^{2+2np-2m-3n} \\
 & \quad + D_1 (1 + np - m - 2n) K_0^{2+2np-2m-4n} \\
 & \quad + B_1 C_1 (1 - n + np - m) K_0^{2+2np-2m-5n} \\
 & \quad - a_0 K_0^{5+4np-4m-6n} - B_1 K_0^{4+4np-4m-6n}] \tag{27}
 \end{aligned}$$

Eq. (25) is valid for all L and B_1 as long as $k_e^{II} > k_{||}$. The range of applicability is limited by the divergence of the Taylor series expansion involved in the solution.

5.3. Cut-off value $k_{||}$

The cut-off value that delimits the small and large k_e solutions can be determined by carefully examining the convergence criteria for the two cases at hand. Based on (14), the requirement for the type-I expansion can be seen to be $|p(\kappa k_e)^n| < 1$. The small series expansion will thus diverge whenever

$$k_e < k_e^+; \quad k_e^+ \equiv |p^{-1/n} \kappa^{-1}| \tag{28}$$

Similarly, the large series expansion of (20) diverges for $|p(\kappa k_e)^{-n}| < 1$ or $k_e > k_e^-; k_e^- \equiv |p^{1/n} \kappa^{-1}|$. The presence of two asymptotic bounds motivates the search for a cut-off $k_{||} \in [k_e^-, k_e^+]$ that can be taken as the simultaneous upper and lower caps for the type-I and type-II approximations. By setting

$$k_{||} = x k_e^- + (1 - x) k_e^+; \quad x \in [0, 1] \tag{29}$$

x is then chosen in a manner to minimize the maximum asymptotic error in both k_e^I and k_e^{II} . After some effort, the optimal value is computed and correlated using a polynomial of the form

$$\begin{aligned}
 x &= s_0 + s_1 \bar{k} + s_2 \bar{k}^2 + s_3 \bar{k}^3 + s_4 \bar{k}^4 \\
 \bar{k} &= 2UL / (k_e^- + k_e^+) \tag{30}
 \end{aligned}$$

where the $s_i = (s_0, s_1, s_2, s_3)$ coefficients are provided in Table 1. These constants are determined using a parametric study involving 2000 runs per geometric shape and a correlation coefficient exceeding 0.998. Using (30), the maximum asymptotic error at the delineation

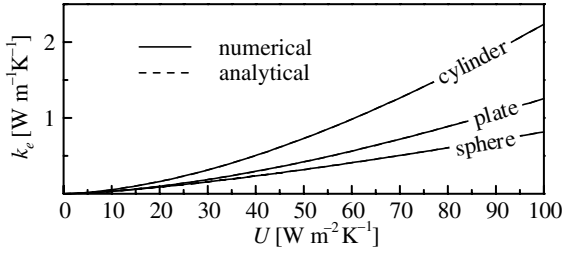


Fig. 2. Numerical verification of the analytical solutions obtained for three geometric shapes and typical operating parameters.

point where both approximations are optimally patched is contained within 2% if k_e is at least 5% away from $k_{||}$. In practice, once the cut-off $k_{||}$ is calculated for a given heat sink application, one may safely use the appropriate correlation depending on the actual operating range:

$$k_e = \begin{cases} k_e^I, & 0 < k_e \leq k_{||} \text{ (laminar regime)} \\ k_e^{II}, & k_e > k_{||} \end{cases} \quad (31)$$

where both approximations are equivalent at the cut-off point. The degree of precision associated with Eqs. (18) and (25) is illustrated in Fig. 2 where analytical and numerical predictions for k_e are compared over a wide range of U and three fundamental configuration shapes.

6. Approximate k_e for laminar and turbulent free convection

For a broader correlation that remains applicable under turbulent conditions, Churchill and Chu [40] have introduced an expression for flow over a flat plate that has also been adopted in diverse physical settings. Theirs can be generically written as

$$Nu_L = UL/k_e = \{a_0 + a_1 Ra^{m/2} [1 + (a_2/Pr)^n]^{p/2}\}^2 \quad (32)$$

Clearly, (32) can be restored from (4) when $q=2$. To make headway, one uses a quadratic expansion to expose individual exponents via

$$UL/k_e = a_0^2 + 2a_0a_1Ra^{m/2}[1 + (a_2/Pr)^n]^{p/2} + \{a_1Ra^{m/2}[1 + (a_2/Pr)^n]^{p/2}\}^2 \quad (33)$$

Subsequently, one may set $A_2 \equiv (g\beta\Delta TL^3\rho^2C_p/\mu)^{m/2}$ and rearrange (33) into

$$UL = a_0^2k_e + 2a_0a_1k_e^{1-m/2}A_2\{1 + [a_2k_e/(\mu C_p)]^n\}^{p/2} + a_1^2k_e^{1-m}A_2^2\{1 + [a_2k_e/(\mu C_p)]^n\}^p \quad (34)$$

From (34) a solution for k_e must be carefully obtained based on the size of U . As usual, two asymptotic approximations can be constructed for small and large U .

6.1. Type I: Dual regime, small U case

To ensure convergence to the desired solution $k_e \approx k_0 + k_1$, we first put $w = [a_2k_e/(\mu C_p)]^n$ into (34). This yields

$$UL = a_0^2k_e + 2a_0a_1A_2k_e^{1-m/2}T_1 + a_1^2A_2^2k_e^{1-m}T_2 \quad (35)$$

where

$$\begin{aligned} T_1 &= 1 - \frac{1}{2}pw + \frac{1}{8}p(p-2)w^2 + \dots \\ T_2 &= 1 - pw + \frac{1}{2}p(p-1)w^2 + \dots \end{aligned} \quad (36)$$

At this point the powers of k_e can be exposed by inserting (36) into (35). One gets

$$\begin{aligned} UL &= a_0^2k_e + 2a_0a_1A_2[k_e^{1-m/2} - \frac{1}{2}puk_e^{1-m/2+n} \\ &\quad + \frac{1}{8}p(p-2)u^2k_e^{1-m/2+2n}] + a_1^2A_2^2[k_e^{1-m} - puk_e^{1-m+n} \\ &\quad + \frac{1}{2}p(p-1)u^2k_e^{1-m+2n}] \\ u &\equiv (a_2/\mu C_p)^n \end{aligned} \quad (37)$$

For the specific constants (m, n, p) listed in Table 1, the leading-order term for this solution can be obtained following Brucker and Majdalani [44]. The result is $k_0 = a_1^{-2/(1-m)}A_2^{-2/(1-m)}(UL)^{1/(1-m)}$. For $m=1/3$, this yields $k_0 = a_1^{-3}A_2^{-3}(UL)^{3/2}$. The final solution can be obtained from

$$k_e^I = a_1^{-3}A_2^{-3}(UL)^{3/2} + k_1 + k_n \quad (38)$$

$$\begin{aligned} k_1 &= -\frac{3}{2}\left[a_0^2k_0^2 + 2a_0a_1A_2\left(k_0^{11/6} - \frac{8}{27}uk_0^{115/48} + \frac{140}{729}u^2k_0^{71/24}\right)\right. \\ &\quad \left.+ a_1^2A_2^2u\left(\frac{344}{729}uk_0^{67/24} - \frac{16}{27}k_0^{107/48}\right)\right]/(UL) \end{aligned} \quad (39)$$

The higher-order corrections at $n=2, 3, \dots$ can be recovered from the recurrence relation

$$\begin{aligned} k_n &= -\frac{3}{2}k_0k_{n-1}\left[a_0^2 + a_0a_1A_2\left(\frac{5}{3}k_0^{-1/6} - \frac{67}{81}uk_0^{19/48}\right)\right. \\ &\quad \left.+ \frac{1645}{2187}u^2k_0^{23/24}\right] + a_1^2A_2^2u\left(\frac{1849}{2187}uk_0^{19/24} - \frac{59}{81}k_0^{11/48}\right)\right]/(UL) \end{aligned} \quad (40)$$

In [44], a two-term approximation for (38) was found to be sufficiently adequate for problems of practical interest. This was realized by comparing results from the compact model with experimental and detailed numerical simulations. Here too, (38) is valid for all L and A_2 so long as $0 < k_e^I \leq k_{||}$.

6.2. Type II: Dual regime, large U case

In this case, F must be expanded in the reciprocal of (κk_e) . This turns (34) into

$$\begin{aligned} UL &= a_0^2k_e + 2a_0a_1A_2u^{-p/2}k_e^{1-m/2+np/2} \\ &\quad + a_1^2A_2^2u^p k_e^{1-m+np} - pa_1^2A_2^2u^{-p-1}k_e^{1-m-np-n} \end{aligned} \quad (41)$$

As usual, negligible terms are phased out. In seeking the leading-order solution, we include all except for the last term in (41). The problem becomes that of solving

$$\begin{aligned}
 & -c_1 + c_2 k_e^{1-m/2+np/2} + c_3 k_e^{1-m+np} + c_4 k_e = 0 \\
 & c_1 \equiv UL, \quad c_2 \equiv a_1^2 A_2^2 u^p, \quad c_3 \equiv 2a_0 a_1 A_2 u^{p/2}, \quad c_4 \equiv a_0^2
 \end{aligned} \tag{42}$$

In the specific cases listed in Table 1, (42) leads to a cubic, namely $-c_1 + c_2 k_e^{1/3} + c_3 k_e^{2/3} + c_4 k_e = 0$. Using $k_e^{\text{II}} \approx K_0 + K_1$ as before, the root can be exacted from

$$K_0 = (c_1 - c_3 p_1^2 - c_2 p_2) / c_4 \tag{43}$$

where

$$\begin{cases} p_0 \equiv (36c_2c_3c_4 + 108c_1c_4^2 - 8c_3^3 + p_2)^{1/3} \\ p_1 \equiv \frac{1}{6}p_0/c_4 - \frac{2}{3}(3c_2c_4 - c_3^2)/(c_4p_0) - \frac{1}{3}(c_3/c_4) \\ p_2 \equiv 12\sqrt{3}c_4\sqrt{27c_1^2c_4 - c_2^2c_3^2 - 4c_1c_3^3 + 4c_2^3c_4 + 18c_1c_2c_3c_4} \end{cases} \tag{44}$$

In order to account for the small correction associated with the fourth term in (41), one can substitute the result back into the expanded Churchill and Chu correlation and solve for the linear correction term,

$$\begin{aligned}
 K_1 = & -\frac{16}{9}a_1^2A_2^2K_0^{-11/48}u^{-43/27}/(3a_0^2 + 4a_0a_1A_2K_0^{-1/3}u^{-8/27} \\
 & + a_1^2A_2^2K_0^{-2/3}u^{-16/27})
 \end{aligned} \tag{45}$$

Eqs. (43) and (45) are valid for all L and c_i so long as $k_e^{\text{II}} > k_{\parallel}$.

6.3. Cut-off value k_{\parallel}

The cut-off value in the dual regime can be obtained following the lines described above. The difference is that the current solution depends on two Taylor series for each approximation, as opposed to only one. This can be seen by realizing that both expansions in (36) will diverge for small U unless $|\frac{1}{2}puk_e^n| < 1$ and $|puk_e^n| < 1$. Both criteria are fulfilled when $k_e < k_e^+$; $k_e^+ \equiv |(pu)^{-1/n}|$. Here, the large U expansion diverges unless $|\frac{1}{2}pu^{-1}k_e^{-n}| < 1$ and $|pu^{-1}k_e^{-n}| < 1$, thus giving $k_e > k_e^-$; $k_e^- \equiv |(p/u)^{1/n}|$. Once again, the procedure summarized in Eqs. (29) and (30) can be used to determine the optimal k_{\parallel} . After 2000 runs per geometric shape, the coefficients of the best fit polynomial are determined with a correlation coefficient exceeding 0.998. In comparison to the numerical solution, the asymptotic result based on patching both solutions at k_{\parallel} deviates by no more than 2% provided that one is at least 5% away from the delineation point. The final solution is expressible by the piecewise form given by (31),

$$k_e = \begin{cases} k_e^1, & 0 < k_e \leq k_{\parallel} \\ k_e^{\text{II}}, & k_e > k_{\parallel} \end{cases} \tag{46}$$

(dual regime, laminar and turbulent)

7. General forced convection

Numerous empirical correlations are available for predicting forced convection heat transfer from bodies of various shapes. Generally, these correlations can be abbreviated by using generic forms that depend on the flow regime. In particular, one may write

$$Nu_L = \begin{cases} C_1 Re_L^m Pr^n, & \text{laminar} \\ C_1 Re_L^p Pr^q, & \text{turbulent} \end{cases} \tag{47}$$

for which

$$Nu_x = \begin{cases} mC_1 Re_x^m Pr^n, & \text{laminar} \\ pC_1 Re_x^p Pr^q, & \text{turbulent} \end{cases}$$

Based on these two relations for average and local Nusselt numbers, one can integrate for the combined laminar and turbulent flow correlation if the critical Reynolds number Re_{cr} is known for the case at hand. One finds

$$Nu_L = [C_1 Re_L^p - (C_1 Re_{cr}^{p-m} - C_1) Re_{cr}^m] Pr^q, \quad n = q \tag{48}$$

For flow over an isothermal plate, one may use $C_1 = 0.664$, $C_t = 0.037$, $m = 1/2$, $p = 4/5$, $n = q = 1/3$, and $Re_{cr} = 5 \times 10^5$ to verify that $Nu_L = (0.037 Re_L^{4/5} - 871.3) Pr^{1/3}$ [1]. When the base plate is subject to a sufficiently uniform heat flux, only leading coefficients in (47) need to be modified. By setting $C_1 = 0.906$ and $C_t = 0.0385$, the corresponding correlation becomes $Nu_L = (0.0385 Re_L^{4/5} - 754.6) Pr^{1/3}$. It should be noted that in most compact models, an isothermal surface temperature is assumed even in the presence of a uniform heat flux. This is justified by virtue of the small surface area and large conductivity of the base plate.

Ordinarily, regardless of the correlation used for forced convection, determination of the effective thermal conductivity is straightforward. This can be accomplished by setting $Nu_L = UL/k_e$ in (47) and (48) and solving for k_e . The result is

$$k_e = \begin{cases} Re_L^m \mu C_p [UL / (C_1 Re_L^m \mu C_p)]^{1/(1-n)}, & \text{laminar} \\ Re_L^p \mu C_p [UL / (C_1 Re_L^p \mu C_p)]^{1/(1-q)}, & \text{turbulent} \\ \{ UL / [C_1 Re_L^p - (C_1 Re_{cr}^{p-m} - C_1) Re_{cr}^m (\mu C_p)^q] \}^{1/(1-q)}, & n = q, \text{ combined} \end{cases} \tag{49}$$

Eq. (49) is instrumental in determining k_e for several shapes used in forced convection studies. These are summarized in Table 2 and include empirical constants due to Jacob [45]. The latter pertain to planar cross-sections whose correlations collapse into the simple expression

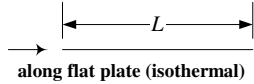
$$Nu_L = C Re_L^m Pr^{1/3} \tag{50}$$

for which

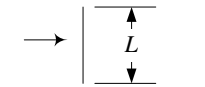
$$k_e = \{ UL / [C Re_L^m (\mu C_p)^{1/3}] \}^{3/2}$$

Table 2
Effective thermal conductivity of common geometric shapes under forced convection

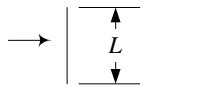
Description	Forced convection correlation	Effective thermal conductivity
1	$Nu_L = 0.664Re_L^{1/2}Pr^{1/3}$	$k_e = \{UL/[0.664Re_L^{1/2}(\mu C_p)^{1/3}]\}^{3/2}$
2	laminar [59] $Nu_L = 0.037(Re_L^{4/5} - 871)Pr^{1/3}$ laminar or turbulent [59]	$Re_L \leq 5 \times 10^5, Pr \geq 0.6$ $k_e = \{UL/[0.037(Re_L^{4/5} - 871)(\mu C_p)^{1/3}]\}^{3/2}$ $5 \times 10^5 \leq Re_L \leq 10^8, 0.6 \leq Pr \leq 60$
3	$Nu_L = 0.906Re_L^{1/2}Pr^{1/3} (\dot{Q} = \text{const})$ laminar [1]	$k_e = \{UL/[0.906Re_L^{1/2}(\mu C_p)^{1/3}]\}^{3/2}$ $Re_L \leq 5 \times 10^5, Pr \geq 0.6$
4	$Nu_L = (0.0385Re_L^{4/5} - 755)Pr^{1/3} (\dot{Q} = \text{const})$ laminar or turbulent [1]	$k_e = \{UL/[0.0385(Re_L^{4/5} - 755)(\mu C_p)^{1/3}]\}^{3/2}$ $5 \times 10^5 \leq Re_L \leq 10^8, 0.6 \leq Pr \leq 60$
5	$Nu_L = 0.2Re_L^{2/3}$ laminar or turbulent, Sogin [60]	$k_e = 5ULRe_L^{-2/3}$ $1 \leq Re_L \leq 4 \times 10^5, Pr = 0.7$
6	$Nu_L = 0.93Re_L^{1/2}Pr^{1/3}$ laminar or turbulent, Tien and Sparrow [61]	$k_e = \{UL/[0.93Re_L^{1/2}(\mu C_p)^{1/3}]\}^{3/2}$ $2 \times 10^4 \leq Re_L \leq 10^5, \text{air}$
7	$Nu_D = 2 + (0.4Re_D^{1/2} + 0.06Re_D^{2/3})Pr^{0.4}(\mu/\mu_s)^{1/4}$ laminar or turbulent, Whitaker [47]	$k_e \rightarrow \text{Eq. (53)}$ $3.5 \leq Re_D \leq 7.6 \times 10^4, 0.7 \leq Pr \leq 380$
8	$Nu_D = 1.05Re_D^{1/2}Pr^{0.36}$ turbulent, Sparrow and Geiger [62]	$k_e = \{UD/[1.05Re_D^{1/2}(\mu C_p)]\}^{1.563}$ $5 \times 10^3 \leq Re_D \leq 5 \times 10^4, 0.7 \leq Pr \leq 380$
9	$Nu_D = 0.591Re_D^{0.564}Pr^{1/3}$ laminar or turbulent, Wedekind [63]	$k_e = \{UD/[0.591Re_D^{0.564}(\mu C_p)]\}^{3/2}$ $9 \times 10^2 \leq Re_D \leq 3 \times 10^4, 0.7 \leq Pr \leq 380$



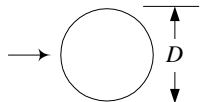
along flat plate (isothermal)



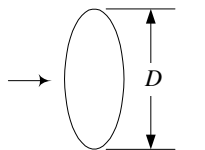
across vertical flat plate



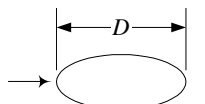
across square plate



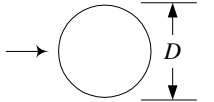
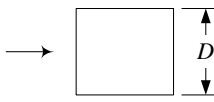
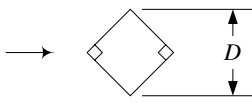
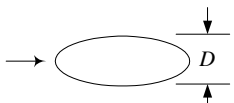
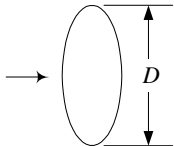
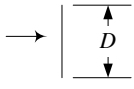
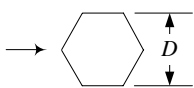
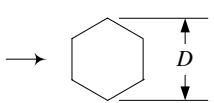
across sphere



across disk



along disk

	Geometry [45]	C	n	Range
10		0.989	0.330	$0.4 < Re_D < 4$
11		0.911	0.385	$4 < Re_D < 40$
12		0.683	0.466	$40 < Re_D < 4 \times 10^4$
13		0.193	0.618	$4 \times 10^4 < Re_D < 4 \times 10^5$
14		0.0266	0.805	$4 \times 10^5 < Re_D < 4 \times 10^6$
15		0.104	0.675	$5 \times 10^4 < Re_D < 1 \times 10^6$
16		0.180	0.699	$2.5 \times 10^4 < Re_D < 8 \times 10^4$
17		0.251	0.588	$5 \times 10^4 < Re_D < 1 \times 10^6$
18		0.293	0.624	$2.5 \times 10^4 < Re_D < 7.5 \times 10^4$
19		0.252	0.612	$2.5 \times 10^4 < Re_D < 1.5 \times 10^5$
20		0.096	0.804	$3 \times 10^4 < Re_D < 1.5 \times 10^5$
21		0.232	0.731	$4 \times 10^4 < Re_D < 1.5 \times 10^5$
22		0.156	0.638	$5 \times 10^4 < Re_D < 1 \times 10^6$
23		0.163	0.638	$5 \times 10^4 < Re_D < 1 \times 10^6$
24		0.039	0.782	$1.95 \times 10^5 < Re_D < 1 \times 10^6$

It may be instructive to note that, for flow over a flat plate, the special equation used in a recent study by Narasimhan and Majdalani [27,28] or Narasimhan et al. [37] can be restored from (49). In these studies, results based on (49) were shown to fall within $\pm 7\%$ of both computational and experimental measurements.

8. Approximate k_e for laminar and turbulent forced convection across a sphere

Some correlations exist for which a standalone diffusivity constant is added to the term containing the Prandtl number. An illustrative case arises in the context of a laminar or turbulent flow across a sphere of diameter D . This form of the equation applies to the natural convection correlation proposed by Yuge [46] for laminar heat transfer from a sphere. The pertinent Nusselt number relation has been developed by Whitaker [47] over the range $3.5 \leq Re_D \leq 7.6 \times 10^4$ and $0.7 \leq Pr \leq 380$. It exhibits the form

$$\begin{aligned} Nu_D &= C_0 + C_1 Pr^n \\ n &\equiv 2/5, \quad C_0 \equiv 2 \\ C_1 &\equiv (0.4 Re_D^{1/2} + 0.06 Re_D^{2/3})(\mu/\mu_s)^{1/4} \end{aligned} \quad (51)$$

where both C_0 and C_1 are independent of k_e . Eq. (51) can be rearranged into

$$\begin{aligned} k_e + Ak_e^m - B &= 0 \\ m &\equiv 1 - nA \equiv (\mu C_p)^n (C_1/C_0), \quad B \equiv UD/C_0 \end{aligned} \quad (52)$$

then solved asymptotically. Since all physical problems exhibit $0 < n < 1$, a reasonably accurate two-term expansion can be obtained from

$$\begin{cases} Ak_0^m - B = 0, & k_0 \text{ small} \\ K_0 - B = 0, & K_0 \text{ large} \end{cases} \quad \text{or} \quad k_e = \begin{cases} \frac{m}{1/B + m(A/B)^{1/m}}, & k_e \leq k_{||} \\ B[1 - 1/(m + B^{1-m}/A)], & k_e > k_{||} \end{cases} \quad (53)$$

where the maximum error remains bounded within $\pm 9.1\%$ for $n \leq 0.4$. The delimiting value for the small range is $k_{||} = (0.08 + 0.727m - 0.314m^2)A$. For $0 < n \leq 0.4$, the error remains bounded within $\pm 2.5\%$; furthermore, the range for $k_{||}$ reduces to $0.40 \leq k_{||}/A < 0.50$.

9. Other correlations

The analytical expressions obtained in the preceding sections enable us to provide direct estimates for k_e in diverse physical settings. This is due to the foregoing generalizations being applicable to a considerable number of flow regimes and geometric configurations.

Exact or approximate solutions for k_e can now be instantly determined for a number of geometric shapes starting with the widely used flat plate model. Based on their fundamental correlations found in the literature, these different cases have been compiled and included in Tables 1 and 2 for free and forced convection, respectively. It should be noted that some common shapes exhibit multiple correlations depending on the choice of coolant and characteristic ranges. Of particular use to compact models are flows along or across arbitrarily inclined flat plates, disks, and squares. Circular cross-sections become suitable, for instance, when tube-mounted heat sinks are being considered. When a three-dimensional component is being cooled from all sides, three-dimensional objects such as tetrahedrons and spheroids may be resorted to. Although some models may not be immediately essential to ongoing industrial designs, they can still hold value in the rapidly growing research into advanced cooling technologies. This is especially true in view of current trends to explore 'shelf technologies' that provide thermal analysts with the valuable and much needed lead-time for future implementation. Since the k_e -value associated with longitudinal flow over a flat plate has been previously validated under free and forced convection conditions, it is hoped that the results derived for other configurations will be tried in future tests.

10. Closing remarks

In this article, several analytical expressions are derived for k_e . These explicit solutions embody many possible heat pathways and base plate geometries that arise in microelectronic packages. From a physical standpoint, the effective thermal conductivity represents a figure-of-merit that assumes an intermediate value greater than that of the coolant ($0.026 \text{ W m}^{-1} \text{ K}^{-1}$ for air), and smaller than that of the metal ($240 \text{ W m}^{-1} \text{ K}^{-1}$ for aluminum and $400 \text{ W m}^{-1} \text{ K}^{-1}$ for copper). In forced convection studies, k_e typically varies between 8 and $16 \text{ W m}^{-1} \text{ K}^{-1}$. However, it can be smaller than unity under natural convection conditions. In principle, the sole purpose of using a lumped thermal concept has been to provide an expedient approach in modeling populated chip packages. In some research circles, the efficacy of compact models in predicting temperature distributions has made them indispensable to the efficient development of competitive packaging designs. Ultimately, lumped thermal models may be needed not just for compact heat sink representations, but also for other components used in electronic enclosures. These may include combinations of heat sinks and other emerging technologies that are currently underway.

Acknowledgement

This project was sponsored partly by the National Science Foundation and partly by the Jack D. Whitfield Professor of High Speed Flows, University of Tennessee.

References

- [1] Y.A. Çengel, Heat Transfer: A Practical Approach, McGraw-Hill, New York, 1998.
- [2] A. Bar-Cohen, A.D. Kraus, Advances in Thermal Modeling of Electronic Components and Systems, vol. 2, ASME Press, New York, 1990.
- [3] W.M. Kays, A.L. London, Compact Heat Exchangers, second ed., McGraw-Hill, New York, 1964.
- [4] D.B. Tuckerman, R.E. Pease, High-performance heat sinking for VLSI, IEEE Electron. Device Lett. 2 (1981) 126–129.
- [5] N. Goldberg, Narrow channel forced air heat sink, IEEE Trans. Comp. Hybrids Manuf. Technol. 1 (1984) 154–159.
- [6] S. Sasaki, T. Kishimoto, Optimal structure for micro-groove cooling fin for high power LSI devices, Electron. Lett. 22 (1986) 1332–1334.
- [7] L.T. Hawang, I. Turluk, A. Reisman, A thermal module design for advanced packaging, J. Electron. Mater. 16 (1987) 347–355.
- [8] D. Nayak, L.T. Hawang, I. Turluk, A. Reisman, A high-performance thermal module for computer packaging, J. Electron. Mater. 16 (1987) 357–364.
- [9] R.J. Phillips, Microchannel heat sinks, in: A. Bar-Cohen, A.D. Kraus (Eds.), Advances in Thermal Modeling of Electronic Components and Systems, vol. 2, ASME Press, New York, 1990 (Chapter 3).
- [10] S. Gavali, S.V. Patankar, K.C. Karki, K. Miura, Effect of heat sink on forced convection cooling of electronic components: a numerical study, Adv. Electron. Pack. 4 (1993).
- [11] M.A. Butterbaugh, S.S. Kang, Effect of airflow bypass on the performance of heat sinks in electronic cooling, Adv. Electron. Pack. 10 (1995) 846–848.
- [12] J.A. Visser, P. Gauche, A computer model to simulate heat transfer in heat sinks, in: Proceedings of the Fourth International Conference for Advanced Computational Methods in Heat Transfer, Udine, 1996, pp. 105–114.
- [13] A. Bar-Cohen, Air-cooled heat sinks—trends and future directions, Adv. Electron. Pack. 19 (1997).
- [14] K. Azar, R.S. McLeod, R.E. Caron, Narrow channel heat sink for cooling of high powered electronic components, in: Eighth IEEE SEMI-THERM Symposium, 1992, pp. 12–19.
- [15] P.R. Souza Mendes, W.F.N. Santos, Heat-transfer and pressure drop experiments in air-cooled electronic component arrays, AIAA J. Thermophys. Heat Transfer 1 (1987) 373–378.
- [16] M.R. Vogel, Thermal performance of air-cooled hybrid heat sinks for a low velocity environment, in: Tenth IEEE SEMI-THERM Symposium, 1994, pp. 17–22.
- [17] R.A. Wirtz, W. Chen, R. Zhou, Effects of flow bypass on the performance of longitudinal fin heat sinks, ASME J. Electron. Pack. 116 (1994) 206–211.
- [18] A. Bar-Cohen, T. Elperin, R. Eliasi, qjc characterization of chip packages—justification, limitations, and future, IEEE Trans. Comp. Hybrids Manuf. Technol. 12 (1989) 724–731.
- [19] W. Krueger, A. Bar-Cohen, Thermal characterization of a PLCC-expanded Rjc methodology, IEEE Trans. Comp. Hybrids Manuf. Technol. 15 (1992) 691–698.
- [20] J.R. Culham, M.M. Yovanovich, S. Lee, Thermal modeling of isothermal cuboids and rectangular heat sinks cooled by natural convection, in: Concurrent Engineering and Thermal Phenomena Proceedings of the Intersociety Conference on Thermal Phenomena in Electronic Systems, vol. 94CH3340, Piscataway, NJ, 1994, pp. 73–82.
- [21] J.R. Culham, M.M. Yovanovich, S. Lee, Thermal modeling of isothermal cuboids and rectangular heat sinks cooled by natural convection, IEEE Trans. Comp. Pack. Manuf. Technol. 18 (1995) 559–566.
- [22] R.L. Linton, D. Agonafer, Coarse and detailed CFD modeling of a finned heat sink, IEEE Trans. Comp. Pack. Manuf. Technol. 18 (1995) 517–520.
- [23] C.D. Patel, C.L. Belady, Modeling and metrology in high performance heat sink design, in: IEEE Electron. Comp. Technol. Conf., Phoenix, AZ, 1997, pp. 296–302.
- [24] C.D. Patel, C.L. Belady, Modeling and Metrology in High Performance Heat Sink Design, Hewlett Packard Laboratories, Palo Alto, CA, 1997.
- [25] S. Kim, S. Lee, On heat sink measurement and characterization, in: IPACK, vol. INTERPACK'97, Hawaii, 1997, pp. 1903–1909.
- [26] S. Narasimhan, B. Kusha, Characterization and verification of compact heat sink models, Proc. Heat Trans. Fluid Mech. Inst. (1998) 43–46.
- [27] S. Narasimhan, J. Majdalani, Characterization of compact heat sink models in natural convection, in: IPACK, vol. 2001-15889, Kauai, Hawaii, 2001.
- [28] S. Narasimhan, J. Majdalani, Characterization of compact heat sink models in natural convection, IEEE Trans. Comp. Pack. Manuf. Technol. 25 (2002) 78–86.
- [29] J.A. Andrews, M. Mahalingam, H. Berg, Thermal characteristics of 16- and 40-pin plastic DIPs, IEEE Trans. Comp. Hybrids Manuf. Technol. 4 (1981) 455–461.
- [30] J.A. Andrews, Package thermal resistance model dependency on equipment design, IEEE Trans. Comp. Hybrids Manuf. Technol. 11 (1988) 528–537.
- [31] M. Mahalingam, Surface-mount plastic packages—an assessment of their thermal performance, IEEE Trans. Comp. Hybrids Manuf. Technol. 12 (1989) 745–752.
- [32] Gautier, Construction and validation of thermal models of packages, in: Seventh IEEE SEMI-THERM Symposium, 1991, pp. 74–79.
- [33] J.P. Le Jannou, Y. Huon, Representation of thermal behavior of electronic components for the creation of a databank, IEEE Trans. Comp. Hybrids Manuf. Technol. 14 (1991) 366–373.
- [34] T.F. Lemczyk, J.R. Culham, S. Lee, M.M. Yovanovich, Fopt—a thermal optimization factor for microelectronic packages, in: Eighth IEEE SEMI-THERM Symposium, 1992, pp. 89–94.

- [35] T.F. Lemczyk, B.L. Mack, J.R. Culham, M.M. Yovanovich, PCB trace thermal analysis and effective conductivity, *J. Electron. Pack.* 114 (1992) 413–419.
- [36] C.J.M. Lasance, H. Vinke, H. Rosten, Thermal characterization of electronic devices with boundary condition independent compact models, *IEEE Trans. Comp. Pack. Manuf. Technol.* 18 (1995) 723–731.
- [37] S. Narasimhan, A. Bar-Cohen, R. Nair, Thermal compact modeling of parallel plate heat sinks, *IEEE Trans. Comp. Pack. Manuf. Technol.* 26 (2003) 136–146.
- [38] P. Teertstra, M.M. Yovanovich, J.R. Culham, Pressure loss modeling for surface mounted cuboid-shaped packages in channel flow, *IEEE Trans. Comp. Pack. Manuf. Technol.* 20 (1997) 463–469.
- [39] S. Narasimhan, A. Bar-Cohen, R. Nair, Flow and pressure field characteristics in the porous block compact modeling of parallel plate heat sinks, *IEEE Trans. Comp. Pack. Manuf. Technol.* 26 (2003) 147–157.
- [40] S.W. Churchill, H.H.S. Chu, Correlating equations for laminar and turbulent free convection from a vertical plate, *Int. J. Heat Mass Transfer* 18 (1975) 1323–1329.
- [41] A.D. Kraus, A. Bar-Cohen, *Thermal Analysis and Control of Electronic Equipment*, Hemisphere, New York, 1983.
- [42] S.W. Churchill, R.U. Churchill, A comprehensive correlating equation for heat an component transfer by free convection, *AIChE J.* 21 (1975) 604–606.
- [43] G. Cardano, *The Rules of Algebra*, Dover, New York, 1993.
- [44] K. Brucker, J. Majdalani, Effective thermal conductivity for compact heat sink models based on the Churchill and Chu correlation, *IEEE Trans. Comp. Pack. Manuf. Technol.* 26 (2003) 158–164.
- [45] M. Jakob, *Heat Transfer*, vol. 1, John Wiley, New York, 1949.
- [46] T. Yuge, Experiments on heat transfer from spheres including combined natural and forced convection, *J. Heat Trans.* 82 (1960) 214–220.
- [47] S. Whitaker, Forced convection heat transfer correlations for flow in pipes, past flat plates, single cylinders, single spheres, and for flow in packed beds and tube bundles, *AIChE J.* 18 (1972) 361–371.
- [48] W.H. McAdams, *Heat Transmission*, third ed., McGraw-Hill, New York, 1954.
- [49] C.Y. Warner, V.S. Arpaci, An experimental investigation of turbulent natural convection in air at low pressure, *Int. J. Heat Mass Transfer* 11 (1968) 397–406.
- [50] E.R.G. Eckert, T.W. Jackson, Analysis of turbulent free convection boundary layer on a flat plate, NASA Technical No. NACA 1015, 1951.
- [51] J.R. Lloyd, W.R. Moran, Natural-convection adjacent to horizontal surface of various planforms, *J. Heat Transfer* 96 (1974) 443–447.
- [52] T. Fujii, H. Imura, Natural convection heat transfer from a plate with arbitrary inclination, *Int. J. Heat Mass Transfer* 15 (1972) 755–767.
- [53] S.W. Churchill, Free convection around immersed bodies, in: K.J. Bell (Ed.), *Heat Exchanger Design Handbook*, Hemisphere, Washington, DC, 1983.
- [54] M.M. Yovanovich, On the effect of shape, aspect ratio and orientation upon natural convection from isothermal bodies of complex shapes, in: Y. Jaluria, R.S. Figliola, M. Kaviany (Eds.), *Convective Transport*, HTD-Vol. 82, ASME, 1987, pp. 121–129.
- [55] S.W. Churchill, H.H.S. Chu, Correlating equations for laminar and turbulent free convection from a horizontal cylinder, *Int. J. Heat Mass Transfer* 18 (1975) 1049–1053.
- [56] V.T. Morgan, *The Overall Convective Heat Transfer from Smooth Circular Cylinders*, vol. 11, Academic Press, New York, 1975.
- [57] M. Al-Arabi, M. Khamis, Natural convection heat transfer from inclined cylinders, *Int. J. Heat Mass Transfer* 25 (1982) 3–15.
- [58] P.H. Oosthuizen, E. Donaldson, Free convection heat transfer from vertical cones, *J. Heat Transfer* 94 (1972) 330–331.
- [59] E.R.G. Eckert, Engineering relations for heat transfer and friction in high-velocity laminar and turbulent boundary layer flow over surfaces with constant pressure and temperature, *Trans. ASME* 78 (1956) 1273–1284.
- [60] H.H. Sogin, A summary of experiments on local heat transfer from the rear of bluff obstacles to a low-speed airstream, *ASME J. Heat Transfer* 86 (1964) 200–202.
- [61] K.K. Tien, E.M. Sparrow, Local heat transfer and fluid flow characteristics for airflow oblique or normal to a square plate, *Int. J. Heat Mass Transfer* 22 (1979) 349–360.
- [62] E.M. Sparrow, G.T. Geiger, Local and average heat transfer characteristics of a disk situated perpendicular to a uniform flow, *J. Heat Transfer* 107 (1985) 321–326.
- [63] G.L. Wedekind, Convective heat transfer measurement involving flow past stationary circular disks, *J. Heat Transfer* 111 (1989) 1098–1100.